ARTICLE

Hierarchy of Relaxation Times in Supramolecular Polymer Model Networks

Received 00th January 20xx,
Accepted 00th January 20xx

DOI: 10.1039/x0xx00000x

Martha Franziska Koziol,*[a] Phuong Loan Nguyen,[a] Shannon Gallo[a], Bradley D. Olsen[b], and Sebastian Seiffert[a]

Supramolecular polymer gels are an evolving class of soft materials with a vast number of properties that can be tuned to desired applications. Despite continous advances concerning polymer synthesis, sustainability or adaptability, a consistent understanding of the interplay between structure, dynamics, and diffusion processes within transient networks is lacking. In this study, the hierarchy of several relaxation processes is investigated, starting from a microscopic perspective of a single sticker dissociation event up to the center-of-mass diffusion of a star-shaped polymer building block on different length scales, as well as the resulting macroscopic mechanical response to applied external stress. In addition to that, a second focus is placed on the gel micro-structure that is analyzed by light scattering. Conversion of the dynamic light scattering (DLS) inverse length scale into real space allows for a combination of relaxation times with those obtained by forced Rayleigh scattering (FRS). For these investigations, a model-type metallo-supramolecular network consisting of narrowly dispersed tetra-arm poly(ethylene glycol)-terpyridine macromolecules that are interconnected via complexation with zinc ions is chosen. Assembling the obtained activation energies reveals that all complex dissociation-governed relaxation processes exhibit similar activation energies.

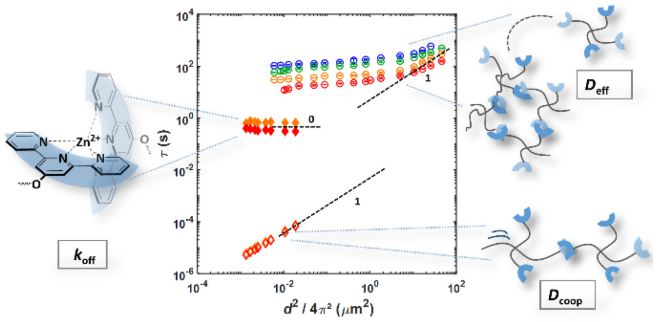

Introduction

Polymer networks consisting of macromonomers with reversible cross-links (also denoted as stickers) are an evolving class of materials exhibiting promising properties due to their dynamic nature. Most of these materials are considered as self-healable[1] and find applications in various fields such as biomedicine[2] or electronics.[3] The dynamic properties of such transient networks are not only influenced by the type and strength of their cross-links (hydrogen bonds, metal–ligand–association, $\pi\pi$-stacking) and external stimuli (pH, temperature, or light)[4] but also by the position of the sticky groups (end-functionalization vs. side-chain-sticker) and the macromonomer architecture (linear vs. stars).[5] In this regard, the approach of developing highly functional materials with tailor-made mechanical properties requires a profound understanding of the underlying dynamic processes. Although many investigations have been conducted over the past two decades, predictions of a supramolecular network's performance starting from the properties of its molecular components (e.g. macromonomers) remains challenging.[6] The complex interplay between the network topology, sticker lifetime(s), and polymer chain dynamics necessitates the use of various complementary characterization techniques to cover both a broad time window as well as an extensive spatial resolution.

Recently, Tang *et al.*[7] revealed a spectrum of several relaxation times that are involved in the total relaxation dynamics of their supramolecular system consisting of linear chains with evenly distributed sticky groups. Like many others,[8,9] they found that the sticker dissociation in the dilute limit is faster than the network exchange time measured by classical rheology. This finding can be explained by the predictions of the sticky Rouse model where a re-normalized bond lifetime τ_b^* has been introduced, showing that a sticker needs several attempts of dissociation and re-association before it can effectively liberate and find a new partner and thereby contribute to stress relaxation.[10]

[a] Department of Chemistry, Johannes Gutenberg-Universität Mainz, Duesbergweg 10-14, D-55128 Mainz, Germany. E-mail: sebastian.seiffert@uni-mainz.de
[b] Department of Chemical Engineering, Massachusetts Institute of Technology, 77 Massachusetts Avenue, Cambridge, Massachusetts 02139, United States

Electronic Supplementary Information (ESI) available: [details of any supplementary information available should be included here]. See DOI: 10.1039/x0xx00000x

On top of that, an unexpected superdiffusive regime has been found in several types of associative networks including protein-based hydrogels,[11] synthetic polymer gels with extremely high sticker density,[12] or star-PEG-terpyridine gels.[13] For explanation, a two-state model has been implemented that is able to phenomenologically describe these anomalous diffusion properties. However, it does not a provide physically meaningful model framework nor meaningful assessment of microscopic variables. As a complement, a molecular model presented by Ramirez *et al*.,[14] introduces several diffusion mechanisms such as walking or hopping, with the latter being the main origin of the superdiffusive regime. By this model, real physical parameters are obtained, but the predictions overestimate several parameters such as the polymer radius of gyration by an order of magnitude. Very recently,[15] Rao and coworkers combined forced Rayleigh scattering (FRS) and neutron spin echo measurements on protein hydrogels to connect segmental polymer strand relaxations with the self-diffusion of the network components, thereby spanning a huge length scale that ranges from nanometers to several micrometers. They found at least two length-scale dependent superdiffusive regimes that reflect a multitude of relaxation mechanisms and molecular states.

In this study, we aim to further understand and compare the hierarchy of characteristic relaxation times coming along with the formation of a model type metallo-supramolecular polymer network transiently built by narrowly dispersed star-shaped poly(ethylene glycol) building blocks.

UV-Vis measurements at dilute conditions, oscillatory shear rheology, and light scattering are chosen as suitable methods to access a wide range of characteristic experimental time and length scales. Our investigations are further completed by forced Rayleigh scattering that provides valuable insights into self-diffusivities on a broad length scale. The combination of these different but yet synergistic characterization techniques allows us to transfer knowledge gained from the isolated macromonomer in solution to the whole network and connect structural as well as dynamic properties.

Experimental

Materials

Commercially available hydroxyl-terminated tetra-arm poly(ethylene glycol) with molar masses of 10,000 g mol^{-1} and 20,000 g mol^{-1} (further denoted as 10k and 20k) was purchased by JenKem® (TX, USA) and re-precipitated before further use. Uvasol® *N*,*N*-Dimethlyformamid Supelco® was used for all spectroscopic assessments.

Scheme 1. Reaction scheme for the synthesis of 4´-[2-(1-Methoxyethoxy)ethoxy]2,2´:6´,2´´-terpyridine (**1**).

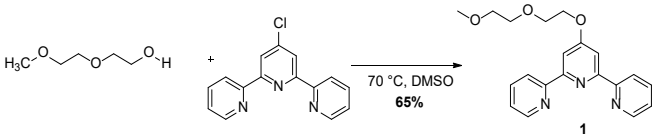

Low molecular terpyridine-model compound. 4´-[2-(1-Methoxyethoxy)ethoxy]2,2´:6´,2´´-terpyridine (**1**) was chosen as a low-molecular model compound for the UV-Vis based determination of the complex dissociation constant in DMF.[16] The reaction route is depicted in Scheme 1.

0.13 g mortared KOH (2.3 mmol, 2.8 eq.) was dried under vacuum overnight in a septum–sealed flask, and, after the drying procedure, 10 mL of dry DMSO was added to the flask. 1 mL of diethylene glycol monomethyl ether (5.15 mmol, 6.36 eq.) was added via syringe, and the reaction mixture was heated to 70 °C for 1 hour. 0.217 g 4´-chloro-2,2´:6´,2´´-terpyridine (0.81 mmol, 1 eq.) was added, and the reaction was stirred overnight at 70 °C. After cooling the flask to room temperature, the reaction mixture was concentrated by short-path vacuum distillation. By dropwise precipitation of the distillation bottom product into 50 mL of stirred cold water, the product (1) could be obtained. This slightly yellow raw product was filtered and dried, and for further purification re-dissolved in 1-2 mL DMSO, followed by re-precipitation. After drying, 0.190 g (65%) of a fine white powder was obtained. ^{1}H-NMR ($CDCl_3$) δ = 8.69 (ddd, 2H), 8.61 (dt, 2H), 8.05 (s, 2H), 7.85 (td, 2H), 7.33 (ddd, 2H), 4.42 (m, 2H), 3.94 (m, 2H), 3.76 (m, 2H), 3.59 (m, 2H), 3.40 (s, 3H, methyl-).

Tetra-arm PEG-terpyridine. Terpyridine end-group modified tetra-arm poly(ethylene glycol) (PEG) with molar masses of M_W = 10,000 g mol^{-1} and M_W = 20,000 g mol^{-1} were synthesized according to a previously published procedure.[13,17] As summarized in Scheme 2, commercially available hydroxyl-terminated star-shaped PEG was reacted with mesyl chloride to yield tetra-arm PEG-mesylate that could further be converted with sodium azide to give telechelic azide functionalities. In a subsequent copper-free Huisgen click reaction, propargyl-terpyridine was added to the tetra-arm PEG-azide, and the final product was obtained.

Scheme 2. Reaction scheme for the three-step synthesis of terpyridine end-functionalized tetra-arm PEG.

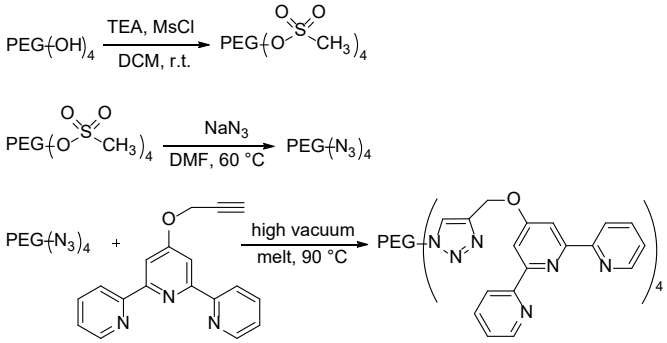

Fluorescence-labeled tetra-arm PEG-terpyridine. In order to obtain self-diffusivities by FRS experiments, tetra-arm polymers that carry both required functional groups, a terpyridine unit and a fluorescent dye on each arm, were synthesized as detailed elsewhere.[13] Briefly, tetra-arm PEG-OH (10,000 g mol^{-1} and 20,000 g mol^{-1}) was reacted with epichlorohydrin to give epoxy-terminated polymers. In a subsequent ring-opening reaction with sodium azide, tetra-arm PEG terminated with an azide and a hydroxyl group was obtained. Terpyridine functionalities were

Scheme 3. Reaction route for the synthesis of terpyridine- and dye-functionalized tetra-arm PEG.

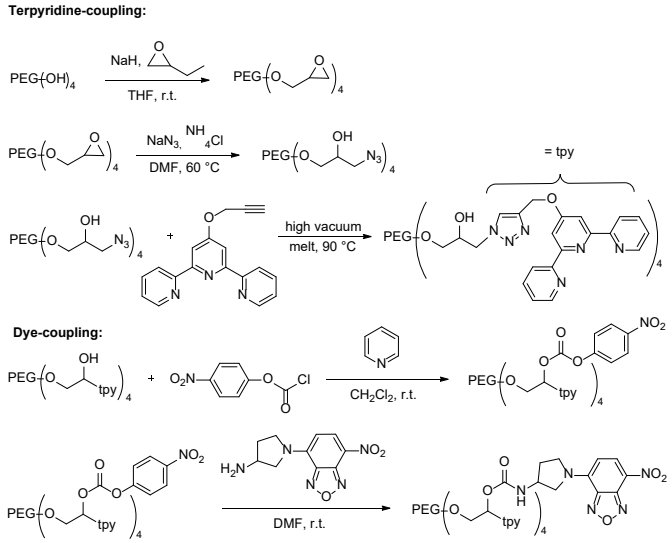

inserted via copper-free click reaction, and, in a following step, the remaining hydroxyl groups were activated with *p*-nitrophenylchloroformate. Further reaction with (*S*)-(+)-4-(3-amino-pyrrolidino)-7-nitrobenzofurazan (NBD) gave the final product (Scheme 3). Excess dye was removed via size exclusion chromatography on a Sephadex LH-20 column in methanol.

Methods

Kinetic measurements based on UV-Vis spectroscopy. To study the bond dissociation kinetics of the zinc-terpyridine complexes, metal exchange experiments in the presence of a twenty-fold molar excess of copper cations were performed. Real-time monitoring of the characteristic metal ligand charge transfer (MLCT) absorption band at 336 nm was carried out on a Jasco V-760-ST spectrophotometer with steady temperatures (10 °C, 15 °C, 20 °C, and 25 °C) assured by a Haake Phoenix II thermostat (Thermo Electron Corporation). All solutions were equilibrated at the desired temperature for 15 minutes before use. 2 mL of a copper nitrate trihydrate solution ($c = 2 \cdot 10^{-4}$ mol L^{-1}) was placed into a UV-Vis cuvette and stirred rigorously. Subsequently, 10 µL of a zinc-terpyridine solution consisting of the low-molecular weight model compound (**1**) and zinc nitrate hexahydrate in a stoichiometric ratio of 2 : 1 (terpyridine : zinc) was quickly added in one shot, and the measurement was started immediately. The final terpyridine concentration was $c = 2 \cdot 10^{-5}$ mol L^{-1}. Assuming pseudo-first order kinetics, the obtained time-dependent absorption curves were fitted to a stretched exponential function (further information in SI).

Gel preparation. The stoichiometric ratio (tpy : zinc) was kept 2 : 1 in all gels. Therefore, the respective amount of a zinc nitrate hexahydrate stock solution in DMF ias quickly added to a solution of tetra-arm PEG-terpyridine in DMF. For FRS experiments, 2% (w/v) of the NBD-labeled species were also added to this mixture. The immediately forming gel was vortexed for 20 s, centrifuged to remove air bubbles, and equilibrated over night at 37 °C. All gels were optically clear.

Rheology. Rheology experiments were performed on an Anton Paar modular compact rheometer type MCR 302 equipped with a cone-plate geometry CP25-1. A gap size of 0.05 µm was chosen, as well as a cone radius of 25 mm and an angle of 1 °. To prevent solvent evaporation, a cooling trap was used. Frequency sweeps were carried out in the linear viscoelastic regime (LVE), applying constant shear rates of γ = 1% and a logarithmic frequency range of ω = 0.01 – 100 rad s^{-1}.

Forced Rayleigh Scattering. The equilibrated samples were loaded between two quartz glass disks that were separated by a Teflon spacer, sealed, and again equilibrated for another day at the desired measurement temperature. Experiments were carried out analogous to a previously detailed procedure.[12,13] In short, a laser beam (cw, 100 mW, λ = 488 nm) that was first split and subsequently focused on the sample with a certain angle θ, created a grating with the characteristic spacing *d*:

$$d = \frac{\lambda}{2 \cdot \sin\left(\frac{\theta}{2}\right)} \quad (1)$$

Due to constructive interference, a short high power bleaching beam with duration of 500–1000 ms created an amplitude grating of dye concentration by irreversibly photobleaching the label on fluorescence-labeled molecules. Molecular diffusion can be monitored by a single attenuated reading beam whose diffraction intensity continuously decreases over time due to the vanishing grating. This decaying intensity $I(t)$ was fit by a slightly stretched exponential function:

$$I(t) = A + B \cdot \exp\left(-\left(\frac{t}{\tau_{FRS}}\right)^{\beta}\right)^2 \quad (2)$$

with the incoherent scattering background *A*, the amplitude *B*, the characteristic relaxation time τ_{FRS}, and the stretch exponent β. The average relaxation time $<\tau_{FRS}>$ was calculated as

$$< \tau_{FRS} > = \frac{\tau_{KWW}}{\beta} \cdot \Gamma\left(\frac{1}{\beta}\right) \quad (3)$$

with Γ being the γ function.

Light scattering. All measurements were carried out on an ALV-SP125-Goniometer, equipped with an ALV/High-QE APD-Avalanche photo diode with fiber optical detection in pseudo cross correlation mode, an ALV 5000/E/PCI correlator, and a JDSU (USA, CA) He/Ne laser (632.8 nm, 35 mW). Angular dependent measurements were performed in a range of 30 °< θ < 150 ° corresponding to wave vectors of $q = (4\pi n \sin(\theta/2)) / \lambda$ with the scattering angle θ, the wavelength λ, and the refractive index $n = 1.42083$ for dimethylformamide (DMF). To account for gel non-ergodicity, scattered light of 500 independent sample positions was recorded using an ALV cuvette rotation unit (CRTU) with a waiting time of 5 s before each measurement and an acquisition time of 30 s (45 °C), 60 s (35 °C), and 90 s (25 °C).

Static Light Scattering. To calculate absolute scattering ratios, the recorded scattering ratio of each gel position was normalized by the ratio of toluene with the Rayleigh ratio $RR = 1.368 \cdot 10^{-5}$ cm^{-1}. Each position-specific ratio is denoted as $<\text{ratio}>_T$, its mean value over all 500 positions corresponds to the ensemble average $<\text{ratio}>_E$. The scattered light of such non-

ergodic systems consists of two contributions: a fluid component <ratio>$_F$ that is mostly position- and angle-independent, and a time-independent excess ratio <ratio>$_{Exc}$, that is caused by frozen static heterogeneities. <ratio>$_F$ is the lower limit of occurring scattering ratios and is obtained by fitting the intensity distribution probability histogram to an exponential decaying function:

$$P(\langle ratio\rangle_T = a \cdot H(\langle ratio\rangle_T - \langle ratio\rangle_F) \cdot \exp\left(-\frac{\langle ratio\rangle_T - \langle ratio\rangle_F}{\langle ratio\rangle_E - \langle ratio\rangle_F}\right) \quad (4)$$

with the Heaviside step function $H = 0$ for (<ratio>$_T$ – <ratio>$_F$) < 0, and $H = 1$ for (<ratio>$_T$ – <ratio>$_F$) ≥ 0. <ratio>$_{Exc}$ can then be calculated by applying <ratio>$_{Exc}$ = <ratio>$_E$ – <ratio>$_F$. If the excess scattering ratio exhibits an angular dependence, it is possible to calculate the static correlation length Ξ that can be seen as a quantitative measure for gel heterogeneity. This is done using a Guinier-type function,[18] where the structure factor $S_{Guinier}$ is approximated by an exponential decay:

$$S_{Guinier} \sim \exp(-q^2 \cdot \Xi^2) \quad (5)$$

The slope of a Guinier plot (ln(<ratio>$_{Exc}$) vs. q^2) then equals Ξ^2.

Dynamic Light Scattering. Due to gel non-ergodicity (ensemble-averaged scattering ratio ≠ time-averaged scattering ratio), partial heterodyne data analysis is chosen to treat the recorded autocorrelation functions.[19,20] A sum of an un-stretched and a stretched exponential decay captures both relaxation processes:

$$g^{(2)}(q,\tau) - 1 = X^2 \cdot g^{(1)}(q,\tau)^2 + 2X \cdot (1-X) \cdot g^{(1)}(q,\tau) = A + \left\{b_{fast} \cdot \exp\left(-\frac{\tau}{\tau_{fast}}\right) + b_{slow} \cdot \exp\left(-\left(\frac{\tau}{\tau_{KWW}}\right)^{\alpha}\right)\right\}^2 \quad (6)$$

with the homodyne scattering contribution $X = \frac{\langle ratio\rangle_F}{\langle ratio\rangle_T}$, the baseline offset A, the amplitudes b_{fast} and b_{slow}, the characteristic relaxation times τ_{fast} and τ_{KWW} and the stretch factor α. The stretched Kohlrausch-Williams-Watts function is chosen to adequately capture the broad distribution of relaxation times (α < 1). The average slow relaxation time τ_{slow} is calculated as

$$\tau_{slow} = \frac{\tau_{KWW}}{\alpha} \cdot \Gamma\left(\frac{1}{\alpha}\right) \quad (7)$$

with the γ function Γ.

The obtained gel diffusion coefficients $D_{Gel,fast} = (q^2\tau_{fast})^{-1}$ exhibit a sample position dependence of the form

$$D_{PHD} = (2 - X) \cdot D_{Gel,fast}, \quad (8)$$

and the collective diffusion coefficient D_{PHD} is then calculated by a linearized expression of equation (8):[20–22]

$$\frac{\langle ratio\rangle_T}{D_{Gel,fast}} = \frac{2}{D_{PHD}} \cdot \langle ratio\rangle_T - \frac{\langle ratio\rangle_F}{D_{PHD}} \quad (9)$$

with the specific speckle ratio <ratio>$_T$ and the fluid ratio <ratio>$_F$. As reported earlier,[21] a weighing factor <ratio>$_T^{-1}$ is used during the linear fitting procedure. The hydrodynamic correlation length ξ_H that can be interpreted as a network mesh size, is calculated via Stokes-Einstein equation (10):

$$\xi_H = \frac{k_B T}{6\pi\eta D_{PHD}} \quad (10)$$

with the Boltzmann constant k_B, the temperature T, and the solvent viscosity η.

Results and Discussion

Two sets of tetra-arm PEG-terpyridine macroprecursors with different molar masses (10,000 g mol^{-1} and 20,000 g mol^{-1}, referred to as 10k and 20k gels when crosslinked in solution) that are transiently connected to percolated networks through complexation with zinc ions, are chosen as the supramolecular material base for our investigations. The samples are probed from molecular (UV spectroscopy), microscopic (light scattering and forced Rayleigh scattering), and macroscopic (rheology) perspectives.

Rheology

Rheology measurements provide insights into the macroscopic material properties manifesting themselves in time-dependent relaxation processes or elastic and viscous contributions of the mechanical response under an external applied stress. A polymer concentration of 10% (wt/v) is chosen for the 10k gels to assure a concentration well below the entanglement limit (c^* for 10k system has been determined to be 9.4% (wt/v).[17] For the 20k gels, a concentration of 20% (wt/v) is chosen to assure an equal sticker concentration when compared to the 10k gels. Figure 1 shows the rheological spectra of the 10k and 20k gels. The frequency-dependent storage and loss modulus (G' and G'') are fitted to a Maxwell-type model that takes into account a distribution of relaxation times (see SI).[23] In general, all 20k gels exhibit slightly higher plateau moduli G_P than the 10k gels. A higher total polymer concentration enhances the probability of interchain bonding instead of elastically inactive intrachain bonding as it might be the case in the 10k gels. Despite different arm lengths, both gel types show nearly the same cross-over frequencies between G' and G'' at the same temperatures, and, as expected, an Arrhenius type temperature dependence if ln($\tau_R^{-1} = k_R$) is plotted vs. T^{-1}. From the slopes of such Arrhenius plots, activation energies are calculated to be (70.91 ± 1.30) kJ mol^{-1} (10k) and (64.44 ± 3.25) kJ mol^{-1} (20k).

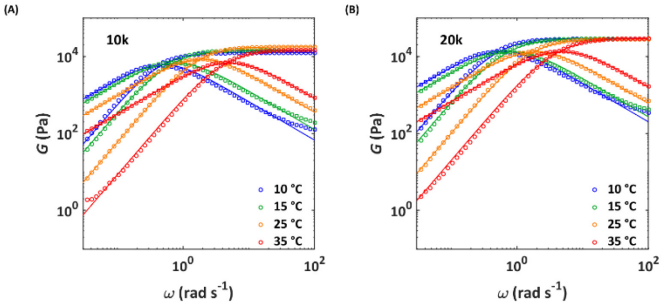

Figure 1. Frequency-dependent rheological spectra of the 10k ((A), M_w = 10,000 g mol^{-1}, 10% (wt/v)) and 20k ((B), M_w = 20,000 g mol^{-1}, 20% (wt/v)) gels at the temperatures of 10 °C, 15 °C, 25 °C, and 35 °C. Fits are shown as straight lines.

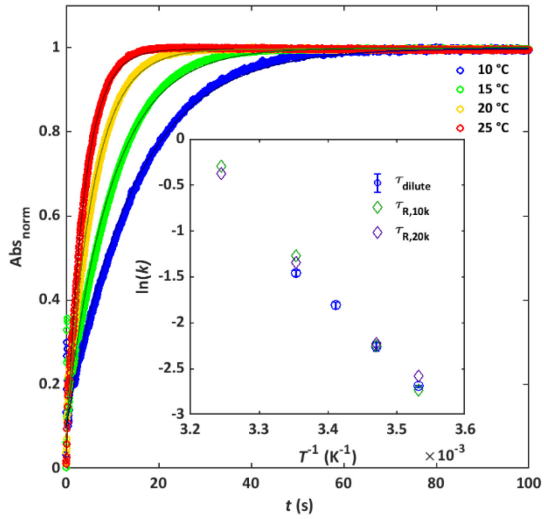

Figure 2. Normalized evolution of the Cu(II)-terpyridine complex MLCT band at 336 nm at different temperatures of 10 °C (blue), 15 °C (green), 20 ° (yellow), and 25 °C (red) in DMF. Inset: Arrhenius plot with combination of UV-Vis kinetics of the low-molecular model compound (**1**) (blue circles) and the cross-over frequencies obtained by rheology (green diamonds (10k) and purple diamonds (20k)).

In addition to the characteristic relaxation times τ_R, the model also provides the standard deviation σ^2 as a quantitative measurement for the width of the relaxation time distribution. Comparison of the gels with different arm lengths shows slightly elevated σ^2-values for the 20k gels and no significant temperature-dependence (Figure S3).

Dilute kinetics

The network relaxation time in transiently connected polymer systems is mainly governed by the kinetics of their single associative junctions.[7] In the tetra-arm PEG-terpyridine networks, the rate-determining step of network rearrangement is the dissociation rate of a zinc terpyridine complex, and it can be investigated by UV-Vis based metal exchange experiments. For this purpose, we synthesized a low-molecular weight model compound (**1**) consisting of a terpyridine group and only two ethylene glycol units attached to it via an oxygen atom to assure similar electronic conditions as in the polymer macromolecules. In our classic metal ion exchange experiment, zinc ions of the low molecular weight model compound-Zn(II)-complexes (**1**) are replaced by stronger binding Cu(II) ions that are present in a 20 fold excess. The terpyridine concentration is kept at $2 \cdot 10^{-5}$ mol L^{-1} in DMF, and the evolution of the characteristic metal ligand charge transfer (MLCT) band at 336 nm is observed. The time-dependent normalized absorbances at four different temperatures are shown in Figure 2.

Fitting these time-traces to an exponential function provides the characteristic dissociation time τ_{dilute} of the zinc terpyridine complex in DMF. We obtain a lower activation energy of $E_{A,dilute} = (58.27 \pm 0.98)$ kJ mol^{-1} compared to our rheology experiments with the 10k and 20k gels ((70.91 ± 1.30) kJ mol^{-1} and (64.44 ± 3.25) kJ mol^{-1}). This finding is explainable if we consider the activation energy obtained by rheology to consist of two additive contributions: the prior dissociation of a zinc terpyridine complex $E_{A,dilute}$ and the subsequent relaxation of the polymer chain $E_{A,polymer}$.[17,24] The inset of Figure 2 shows that the absolute relaxation rates $k_{dilute} = \tau_{dilute}^{-1}$ (blue open circles) are nearly the same as the macroscopic relaxation rates $k_R = \tau_R^{-1}$ measured by rheology (open green and purple diamonds). This finding stays in contrast to a study by Tang and Olsen, where the dilute relaxation time is faster by an order of magnitude compared to the macroscopic relaxation.[7] Identical τ_{dilute} and τ_R values indicate an unexpected negligible effect of bond lifetime renormalization, and are proposed in a model introduced by Stukalin and coworkers[25] only if the associate bond strength (expressed by the activation energy $E_{A,dilute}$) is significantly higher than the restoring energy of a dangling chain (consisting of N monomers) with $2\,RT \ln N$.[9] Our UV-Vis experiments revealed a bond strength of $E_{A,dilute} = (58.27 \pm 0.98)$ kJ mol^{-1},

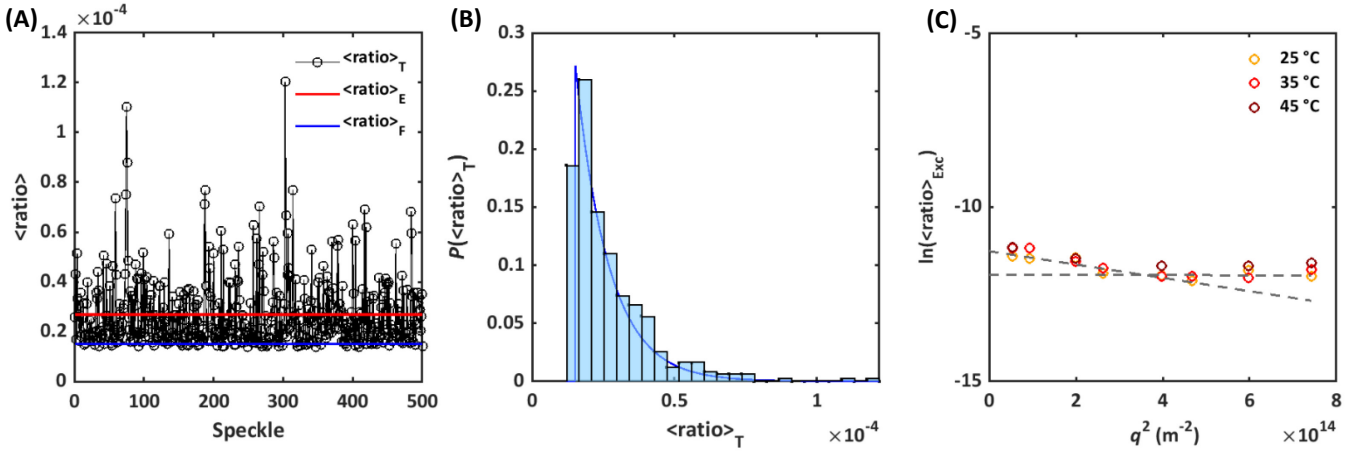

Figure 3. (A) <Ratio>$_T$ speckle pattern of 500 randomly chosen positions within the tetra-arm PEG-terpyridine zinc gel (M_W = 10,000 g mol^{-1}, 10% (w/v), DMF) at an angle of 30 ° and a temperature of T = 25 °C, with the ensemble average <ratio>$_E$ (red line) and the fluid contribution <ratio>$_F$ (blue line). (B) Probability distribution and Heaviside fit (blue line). (C) Guinier plot of all calculated excess ratios <ratio>$_{Exc}$ vs. scattering vector q^2 at three different temperatures 25 °C (yellow symbols), 35 °C (red symbols), and 45 °C (maroon symbols).

whereas the restoring energy of an arm ($M_{w,arm}$ = 2,500 g mol^{-1}, T = 298 K, and $N \cong 56$ for the 10k gel) can be calculated as 2 RT ln N = 19.96 kJ mol^{-1} (23.42 kJ mol^{-1} for 20k).

Light Scattering

Light scattering is a powerful non-invasive technique that is able to provide valuable insights not only into the gel microstructure (static correlation lengths), but also its dynamic processes and hydrodynamic correlation lengths. To complete the picture of hierarchical relaxation times within the supramolecular model networks, simultaneous static and dynamic light scattering experiments (SLS and DLS) on the 10k gel (10% (w/v)) at three different temperatures (25 °C, 35 °C, and 45 °C) are conducted.

Static light scattering

At each temperature, the gel exhibits a typical intensity speckle pattern (Figure 3(A)) with sample-position dependent intensities that compromise scattering contributions from frozen heterogeneities, as well as contributions caused by thermal fluctuations of the polymer chains that are restricted in their motion due to the crosslinks. The latter distinguish themselves by a specific lower cut-off scattering ratio that occurs with the highest probability and is referred to as the fluid ratio <ratio>$_F$. To decompose both scattering contributions, <ratio>$_F$ is obtained by fitting the probability histogram of all measured ratios (Figure 3(B)) with an exponentially decaying function (see experimental part). Figure 4(A) shows no angular dependence of the fluid ratio (open squares) and a slight increase with increasing temperature that can be explained by the enhanced thermal motion of the polymers at higher temperatures. In contrast to that, the overall scattering ratio <ratio>$_E$ shows a distinct angular dependence, especially at lower angles (open circles in Figure 4(A)). The second scattering contributor is the additional excess scattering <ratio>$_{Exc}$ and it is calculated by subtracting the fluid ratio from the ensemble ratio. According to the Guinier approach that treats the gel as a medium consisting of randomly distributed domains with different densities, we calculate temperature-independent static correlation lengths of $\Xi_{25°C}$ = 44 nm, $\Xi_{35°C}$ = 54 nm, and $\Xi_{45°C}$ = 39 nm (Figure 2(C)). Values in a very similar order of magnitude are also reported for non-ideal permanently connected tetra-PEG hydrogels.[26] Even though this transiently connected tetra-arm PEG-terpyridine gel is considered as a dynamic model system with its dissociating and re-associating polymer building blocks, static heterogeneities with density disparities are clearly present. The light scattering results are summarized in Table 1.

Dynamic light scattering

At all measured temperatures, the gel exhibits two distinct relaxation modes. The intensity correlation functions $g^{(2)}(\tau)$ of three out of five hundred randomly chosen positions within the gel are depicted in Figure 5. Similar to earlier studies,[27] the fast mode is assigned to the cooperative segmental relaxation of polymer blobs whereas the slow non-diffusive mode is mainly governed by the network relaxation time. On these short time

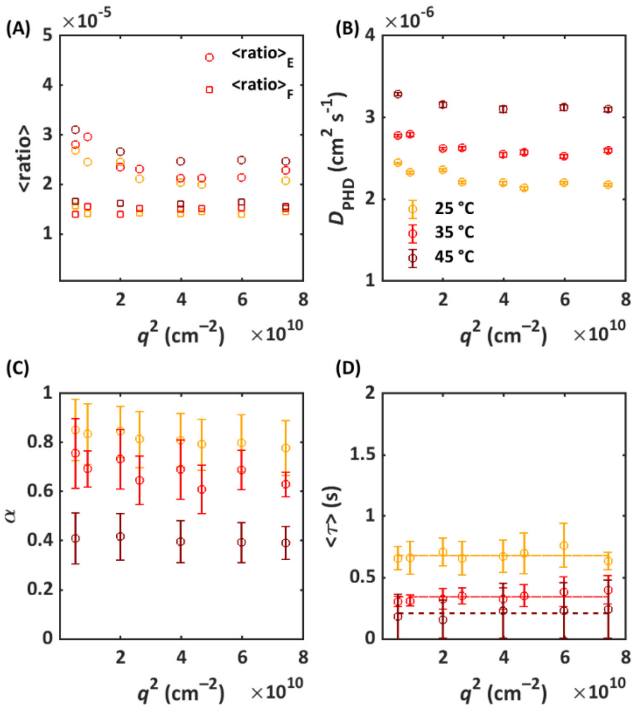

Figure 4. Results of the partial heterodyne data analysis of a zinc tetra-arm PEG-terpyridine gel (DMF, 10% (wt/v)) at three different temperatures (25 °C yellow, 35 °C red, 45 °C maroon). (A) Scattering ensemble ratio (open circles) and fluid ratio (open squares) vs. q^2. Unlike the ensemble ratio, the fluid ratio does not exhibit an angular dependency. (B) Diffusion coefficient D_{PHD} vs. scattering vector q^2. (C) The averaged stretch exponent α is decreasing with increasing temperature. Error bars depict the standard deviation of all 500 positions. (D) Angular-independent relaxation time of the slow relaxation mode occurring at the greatest frequency of all 500 measured times.

scales, the diffusive fast chain motion is decoupled from the viscoelastic network relaxation. The diffusion coefficient D_{PHD} of the fast mode that can be converted into the hydrodynamic correlation length ξ_H, is obtained by partial heterodyne analysis (equation (6)). Plotting $\frac{D_{Gel,fast}}{<ratio>_T}$ vs. <ratio>$_T$ yields a linear dependence with D_{PHD} extracted from the resulting slope (see Figure S5). All calculated diffusion coefficients and hydrodynamic correlation lengths are summarized in Table 1.

Figure 4(B) shows the obtained fast diffusion coefficients vs. scattering vector q^2. Only a slight dependence at low angles is visible. As expected, the diffusion coefficients increase with increasing temperature due to the faster polymer chain motion. Analysis of the q^2-independent slow mode revealed remarkable heterogeneities in the underlying dynamic processes, a fact that is qualitatively illustrated by the strong position-dependence of the correlation function amplitudes (Figure 5(B)). This heterogeneity is quantified by the stretch exponent α as well as the relaxation time <τ>. A stretch exponent below 1 denotes a distribution of relaxation times. Comparison of the stretch exponents of all 500 sample positions of the zinc tetra-arm PEG-terpyridine gel at 25 °C and an angle of 30 ° (Figure S4), reveals a broad distribution ranging from 0.5 to 1. Figure 4(C) depicts the respective average of α depending on the scattering vector

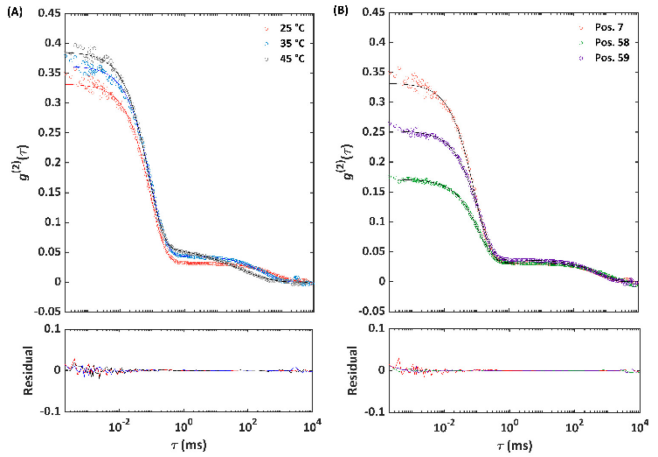

Figure 5. (A) Exemplary intensity correlation functions and fit residuals of a zinc tetra-arm PEG-terpyridine gel (DMF, 10% (w/v)) at three temperatures with fits to the sum of an exponential and a stretched exponential function (lines). (B) Exemplary intensity correlation functions and fit residuals at three randomly chosen gel positions, measured at 25 °C and an angle of 30 °, showing position-dependent variations of the initial q^2 at three different temperatures. With increasing temperature, the stretch exponent decreases to an average value of 0.4. Such low values indicate a very broad distribution of relaxation times. Since these values are unusually low, we tried a fitting procedure with a tri-exponential function, but it did not provide reasonable parameters.

An even broader distribution with relaxation times ranging from 500 ms to 2 s is also found at 25 °C (Figure S5). Analogous to the stretch exponent, the distribution significantly broadens with increasing temperature and as expected, the relaxation time decreases due to faster thermally activated zinc-terpyridine complex exchange. The broad relaxation time distribution that is only detectable in our light scattering experiments could originate from the former found spatial heterogeneities with their significant differences in polymer density. The position-dependent local network relaxation times are strongly affected by the micro-environment of the zinc-terpyridine complexes and the concentration of open stickers in close vicinity to bind to. Further, additional slower diffusive modes with small amplitudes that are not resolvable on the experimental time scales, might influence the slow relaxation time although fitting to a tri-exponential decay does not yield in rational results. Figure 4(D) summarizes the slow relaxation times depending on q^2 and the temperature. We decide to depict the relaxation times with the greatest frequency, because averaging over such a broad distribution is unsubstantiated. Due to this broad distribution, an activation energy of $E_{A,DLS}$ = (48.37 ± 3.60) kJ mol^{-1} with a relatively large uncertainty is calculated. Combination of our static and dynamic light scattering results reveals that the spatial density distribution within the polymer gel exhibits a non-negligible impact on the network dynamics, thereby leading to an unusual broad distribution of relaxation times.

Self-diffusion by FRS

Forced Rayleigh scattering is chosen as a method to investigate the self-diffusivities of fluorescence-labeled tetra-arm PEG-terpyridine macromolecules through the network on length scales of 0.5–24 μm. The relaxation times are obtained by monitoring the Bragg-diffracted beam intensity created by a vanishing sinusoidal dye concentration profile. Similar to previously investigated protein-based P_4-coils[11,15] and linear acrylamide chains with nickel–histidine coordination bonds,[12] a phenomenological superdiffusive regime with $\langle\tau\rangle \sim d^{2\alpha}$ ($\alpha < 1$) is found in a range of d^2 = 0.3–200 μm² in the 10k gels. Beyond this range, terminal Fickian diffusion is observed in all tetra-arm PEG-terpyridine networks at various temperatures (Figure 6(A)).

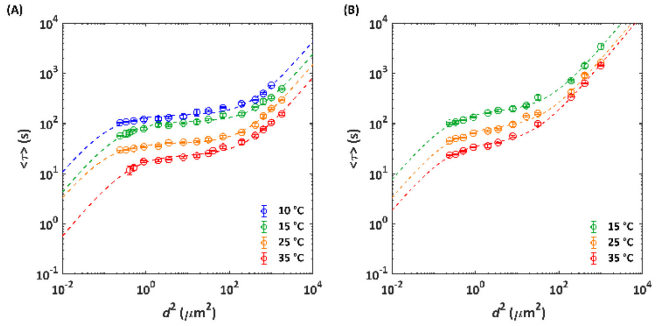

Figure 6. $\langle\tau\rangle$ vs. d^2 of a zinc tetra-arm PEG-terpyridine network ((A): M_w = 10,000 g mol^{-1}, 10% (w/v) and (B): M_w = 20,000 g mol^{-1}, 20% (w/v)) at the temperatures 10 °C (blue), 15 °C (green), 25 °C (yellow), and 35 °C (red) with fits to the two-state model (dashed lines). Error bars depict standard deviations of three different gel position measurements.

As reported earlier,[11,13] the d^2-dependent relaxation times $\langle\tau\rangle$ are fitted to an empirical two-state model that is based on a set of reaction-diffusion equations. (Further explanation and equations can be found in SI). Despite its simplifications and the main assumption of only two existing states, the course of $\langle\tau\rangle$ is captured by the two-state model throughout the whole d^2-range (Figure 6, dashed lines). Figure 7 shows the obtained temperature-dependent fit parameters k_{off} (A), $D_{M,eff}$ (B), and γK_{eq} (C) for the 10k and 20k gels. It should be noted that k_{off} describes the interconversion rate from the stated phenomenological associated to the molecular state. As expected, k_{off} is decreasing with decreasing temperature whereby the 20k gel has lower absolute k_{off} values.

In terms of the model, this finding implies that the interconversion between the molecular and the associated state is faster with decreasing arm length.

Table 1. ξ_H, Ξ, $\langle$ratio$\rangle_F$, $\langle$ratio$\rangle_E$, and D_{PHD} of a zinc tetra-arm PEG-terpyridine gel (10% (w/v), DMF) at three different temperatures (25 °C, 35 °C, and 45 °C).

Temperature	ξ_H (nm)	Ξ (nm)	$\langle$ratio$\rangle_E$ (90 °)	$\langle$ratio$\rangle_F$ (90 °)	D_{PHD} (cm² s^{-1})
25 °C	1.24	44	2.04 · 10^{-5}	1.41 · 10^{-5}	2.20 · 10^{-6}
35 °C	1.10	54	2.13 · 10^{-5}	1.50 · 10^{-5}	2.55 · 10^{-6}
45 °C	0.94	39	2.46 · 10^{-5}	1.61 · 10^{-5}	3.10 · 10^{-6}

ARTICLE

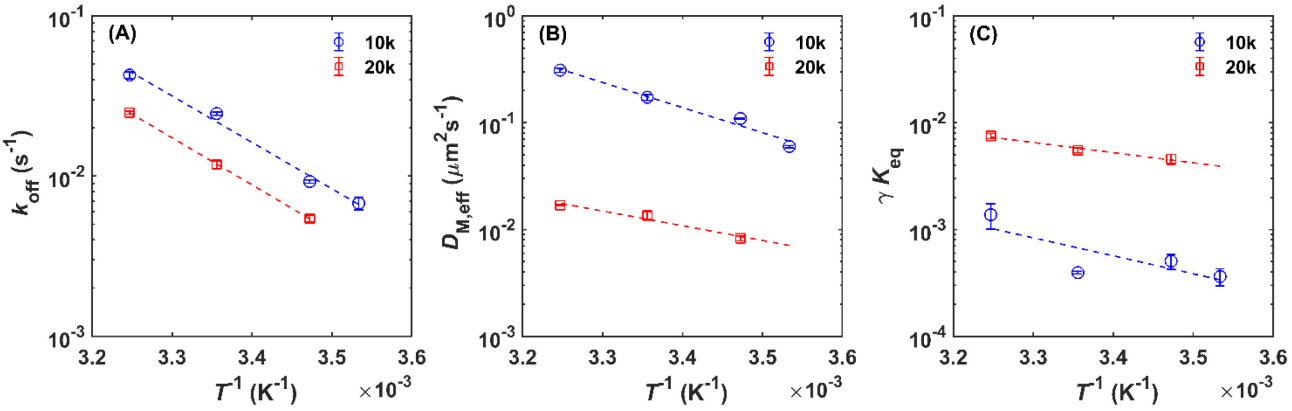

Figure 7. Temperature-dependent two-state model fit parameters k_{off} (A), $D_{M,eff}$ (B), and γK_{eq} (C) of a 10k zinc tetra-arm PEG-terpyridine (10% (w/v), blue symbols) and a 20k zinc tetra-arm PEG-terpyridine (20% (w/v), red symbols) network in DMF.

Even though k_{off} cannot be directly considered to be a physical constant because it is found to have significant concentration dependencies,[11] we obtain the same activation energies of $E_{A,10k}$ = (62.07 ± 4.82) kJ mol^{-1} and $E_{A,20k}$ = (58.13 ± 1.77) kJ mol^{-1} as that obtained by UV-Vis measurements. The activation energy can therefore be considered as independent of arm length and total polymer concentration. The width of the superdiffusive regime is increasing with decreasing temperature and the 20k gels exhibit a less wide superdiffusive regime as expressed by the higher anomaly constant γK_{eq}. The latter fact might result as an effect of the increased total polymer concentration in the 20k gels and the consequentially decreased number of loops, as found earlier in the rheology section. Reduced loop formation would lead to fewer hopping events because more arms are attached to the network, giving a narrower superdiffusive regime.[14] In general, hopping describes the diffusive motion when a star-polymer detaches all four arms from the network and its center-of-mass travels an unexpected large distance. Rapp *et al*.[28] showed that the equilibrium binding constant of a sticker is drastically reduced if other arms of the same molecule are already connected to the network. The chain conformation of an un-attached arm is limited by the surrounding local network structure and binding is therefore entropically unfavoured. They also stated that with increasing chain length, the entropic penalty for binding generally decreases as more chain conformations are possible. We support this finding with our 20k gels where the width of the superdiffusive regime is narrowed by an order of magnitude when compared to the 10k gels.

Recent molecular simulations based on Brownian dynamics of star-shaped polymer networks predict a Fickian regime at low length scales d^2, followed by a caging regime, one (or more) apparent superdiffusive regimes and again, Fickian diffusion at large length scales with an effective diffusivity.[14]

To combine our light scattering and FRS results, the reciprocal length scale q accessed by LS is converted into real space via $d = \frac{2\pi}{q}$. By doing so, we obtain a length scale range between 0.23 µm and 24 µm. Figure 8(A) shows the jointed results. The fast mode obtained by light scattering exhibits a linear $\tau_{fast} \sim d^2$ dependency that is typical for diffusive motion (Figure 8(A), open diamonds). This cooperative chain motion is faster by seven orders of magnitude than the self-diffusion of a single associating star. We achieve an overlap of our FRS and DLS data in a length scale range of $1 \cdot 10^{-2} - 2 \cdot 10^{-2}$ µm². At this intermediate length scale d, the center-of-mass diffusion of

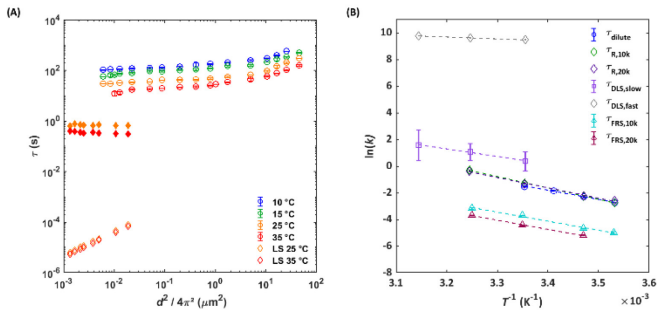

Figure 8. (A) Combination of FRS (open circles) and LS (fast mode: open diamonds, slow mode: closed diamonds) relaxation times vs. real space d^2 of a zinc tetra-arm PEG-terpyridine network (10k, 10% (w/v), in DMF) at 10 C (blue), 15 °C (green), 25 °C (yellow), and 35 °C (red), along with fits to the two-state-model (dashed lines). (B) . Comparison of the characteristic temperature-dependent relaxation times obtained in dilute conditions (blue circles), terminal relaxation times obtained by rheology measurements (green (10k) and purple (20k) diamonds), fast and slow relaxation times obtained by light scattering (grey diamonds and purple squares), and relaxation times obtained by FRS (turquoise (10k) and maroon (20k) triangles) of a zinc tetra-arm PEG-terpyridine gel in DMF.

macromonomers, the collective segmental polymer relaxation, and the sticker dissociation is visible. The self-diffusivities probed by FRS might not be visible in our DLS experiments as the experimental time window cannot adequately capture such a slow relaxation process.

Finally, Figure 8(B) shows a combined Arrhenius plot of all inverse characteristic relaxation times obtained by UV-Vis, rheology, FRS and DLS. Those rate constants span a broad range of 15 orders of magnitude with the fastest rate being the relaxation of single polymer strands between the transiently connected stickers as probed by DLS. For this process, a comparably low activation energy of (11.62 ± 1.12) kJ mol^{-1} is calculated.

As discussed in a previous section, the terminal relaxation times obtained by rheology coincide with the dissociation time of an isolated zinc terpyridine complex in dilute conditions (compare blue circles and green and purple diamonds in Figure 8(B)). Surprisingly, the slow mode that is present in all DLS intensity correlation functions exhibits a slower relaxation time resulting in a higher relaxation rate when compared to rheology or UV-Vis. This finding is striking, as we would expect the dissociation time of the isolated zinc terpyridine complex to be the lower time limit for further emerging viscoelastic relaxation processes. As shown earlier, the unusual broad relaxation time distribution leads to large uncertainties concerning the absolute relaxation time determination. As a lower limit, the slowest times are generated by the center-of-mass diffusion of single star-shaped polymer molecules within the network. Based on our static light scattering results, we cannot exclude relaxation mechanisms through cluster/aggregate diffusion, however, such slow relaxation times are not accessible by the experimental methods used in this work.

Conclusions

A complex hierarchy of relaxation times is studied in telechelic model-type tetra-arm PEG gels that are percolated in solution through transient zinc-terpyridine complexes. In this work, various experimental techniques such as FRS, SLS, DLS, UV-Vis, and rheology are chosen to access broad time and length scale ranges and to combine polymer self-diffusivities, single sticker dissociation times as well as mechanical stress response. In contrast to other linear polymer networks, the star-shaped polymer model network investigated in this study only exhibits a negligible effect of bond lifetime renormalization. The diffusion properties are influenced by the appearance of an anomalous superdiffusive regime that is less pronounced if the polymer arm length is increased (at constant total sticker concentration). A thorough understanding of the supramolecular network dynamics is of major importance to connect the microscopic properties with the resulting macroscopic network performance such as self-healing or permeability. In addition to that, network dynamics are often influenced by the underlying network topology and strongly depend on temperature. Combination of our FRS and LS data shows a multitude of relaxation processes, each with characteristic time and length scale dependencies. In general, these insights might be transferable to other associated polymer systems to help completing the picture of relaxation processes and mechanisms.

Conflicts of interest

There are no conflicts to declare.

Acknowledgements

This work was supported by the German Research Foundation (DFG) under grant no. SE 1888/7-1 (Project no. 376900084). FRS experiments at MIT are supported by NSF DMR-1709315. We would like to sincerely thank Ameya Rao and Irina Mahmad Rasid for advice and valuable discussions concerning FRS. M.F.K. acknowledges Dr. Karl Fischer for constant support.

References

1 a) J. Liu, C. S. Y. Tan, Z. Yu, N. Li, C. Abell and O. A. Scherman, *Advanced materials (Deerfield Beach, Fla.)*, 2017, **29**; b) Q. Zheng, Z. Ma and S. Gong, *J. Mater. Chem. A*, 2016, **4**, 3324–3334; c) T. Yan, K. Schröter, F. Herbst, W. H. Binder and T. Thurn-Albrecht, *Scientific reports*, 2016, **6**, 32356; d) N. Holten-Andersen, A. Jaishankar, M. Harrington, D. E. Fullenkamp, G. DiMarco, L. He, G. H. McKinley, P. B. Messersmith and K. Y. C. Lee, *Journal of materials chemistry. B*, 2014, **2**, 2467–2472; e) K. Varaprasad, G. M. Raghavendra, T. Jayaramudu, M. M. Yallapu and R. Sadiku, *Materials science & engineering. C, Materials for biological applications*, 2017, **79**, 958–971;

2 a) M. J. Webber, E. A. Appel, E. W. Meijer and R. Langer, *Nature materials*, 2016, **15**, 13–26; b) L. Shi, P. Ding, Y. Wang, Y. Zhang, D. Ossipov and J. Hilborn, *Macromolecular rapid communications*, 2019, **40**, e1800837; c) C. O. Akintayo, G. Creusen, P. Straub and A. Walther, *Macromolecules*, 2021; d) T. R. Hoare and D. S. Kohane, *Polymer*, 2008, **49**, 1993–2007;

3 E. W. Meijer and A. P. H. J. Schenning, *Nature*, 2002, **419**, 353–354.

4 J. Hoque, N. Sangaj and S. Varghese, *Macromolecular bioscience*, 2019, **19**, e1800259.

5 M. Golkaram and K. Loos, *Macromolecules*, 2019, **52**, 9427–9444.

6 S. P. O. Danielsen, H. K. Beech, S. Wang, B. M. El-Zaatari, X. Wang, L. Sapir, T. Ouchi, Z. Wang, P. N. Johnson, Y. Hu, D. J. Lundberg, G. Stoychev, S. L. Craig, J. A. Johnson, J. A. Kalow, B. D. Olsen and M. Rubinstein, *Chemical reviews*, 2021, **121**, 5042–5092.

7 S. Tang and B. D. Olsen, *Macromolecules*, 2016, **49**, 9163–9175.

8 a) A. Shabbir, I. Javakhishvili, S. Cerveny, S. Hvilsted, A. L. Skov, O. Hassager and N. J. Alvarez, *Macromolecules*, 2016, **49**, 3899–3910; b) B. J. Gold, C. H. Hövelmann, N. Lühmann, N. K. Székely, W. Pyckhout-Hintzen, A. Wischnewski and D. Richter, *ACS Macro Lett.*, 2017, **6**, 73–77;

9 S. Ge, M. Tress, K. Xing, P.-F. Cao, T. Saito and A. P. Sokolov, *Soft matter*, 2020, **16**, 390–401.

10 M. Rubinstein and Semenov, Alexander, N., *Macromolecules*, 1998, 1386–1397.

11 S. Tang, M. Wang and B. D. Olsen, *Journal of the American Chemical Society*, 2015, **137**, 3946–3957.

12 I. Mahmad Rasid, N. Holten-Andersen and B. D. Olsen, *Macromolecules*, 2021, **54**, 1354–1365.

13 S. Tang, A. Habicht, S. Li, S. Seiffert and B. D. Olsen, *Macromolecules*, 2016, **49**, 5599–5608.
14 J. Ramirez, T. J. Dursch and B. D. Olsen, *Macromolecules*, 2018, **51**, 2517–2525.
15 A. Rao, H. Yao and B. D. Olsen, *Phys. Rev. Research*, 2020, **2**.
16 I. M. Henderson and R. C. Hayward, *Polym. Chem.*, 2012, **3**, 1221.
17 T. Rossow and S. Seiffert, *Polym. Chem.*, 2014, **5**, 3018–3029.
18 a) M. Shibayama, T. Tanaka and C. C. Han, *The Journal of Chemical Physics*, 1992, **97**, 6829–6841; b) S. Mallam, F. Horkay, A. M. Hecht, A. R. Rennie and E. Geissler, *Macromolecules*, 1991, **24**, 543–548; c) S. Seiffert, *Progress in Polymer Science*, 2017, **66**, 1–21;
19 T. Norisuye, Q. Tran-Cong-Miyata and M. Shibayama, *Macromolecules*, 2004, **37**, 2944–2953.
20 J. G. H. Joosten, J. L. McCarthy and P. N. Pusey, *Macromolecules*, 1991, **24**, 6690–6699.
21 M. Shibayama, S.-i. Takata and T. Norisuye, *Physica A: Statistical Mechanics and its Applications*, 1998, **249**, 245–252.
22 M. Shibayama, Y. Fujikawa and S. Nomura, *Macromolecules*, 1996, **29**, 6535–6540.
23 S. C. Grindy, R. Learsch, D. Mozhdehi, J. Cheng, D. G. Barrett, Z. Guan, P. B. Messersmith and N. Holten-Andersen, *Nature materials*, 2015, **14**, 1210–1216.
24 W. Knoben, N. A. M. Besseling and M. A. Cohen Stuart, *The Journal of Chemical Physics*, 2007, **126**, 24907.
25 E. B. Stukalin, L.-H. Cai, N. A. Kumar, L. Leibler and M. Rubinstein, *Macromolecules*, 2013, **46**.
26 Y. Tsuji, S. Nakagawa, C. I. Gupit, M. Ohira, M. Shibayama and X. Li, *Macromolecules*, 2020, **53**, 7537–7545.
27 M. F. Koziol, K. Fischer and S. Seiffert, *Macromolecules*, 2021, **54**, 4375–4386.
28 P. B. Rapp, A. K. Omar, B. R. Silverman, Z.-G. Wang and D. A. Tirrell, *Journal of the American Chemical Society*, 2018, **140**, 14185–14194.